

# High-precision Monte Carlo study of directed percolation in $(d + 1)$ dimensions

Junfeng Wang,<sup>1,2</sup> Zongzheng Zhou,<sup>3</sup> Qingquan Liu,<sup>1</sup> Timothy M. Garoni,<sup>3,\*</sup> and Youjin Deng<sup>1,†</sup>

<sup>1</sup>*Hefei National Laboratory for Physical Sciences at Microscale and Department of Modern Physics, University of Science and Technology of China, Hefei, Anhui 230026, China*

<sup>2</sup>*School of Electronic Science and Applied Physics, Hefei University of Technology, Hefei 230009, China*

<sup>3</sup>*School of Mathematical Sciences, Monash University, Clayton, Victoria 3800, Australia*

(Dated: July 6, 2018)

We present a Monte Carlo study of the bond and site directed (oriented) percolation models in  $(d+1)$  dimensions on simple-cubic and body-centered-cubic lattices, with  $2 \leq d \leq 7$ . A dimensionless ratio is defined, and an analysis of its finite-size scaling produces improved estimates of percolation thresholds. We also report improved estimates for the standard critical exponents. In addition, we study the probability distributions of the number of wet sites and radius of gyration, for  $1 \leq d \leq 7$ .

PACS numbers: 64.60.ah, 05.70.Jk, 64.60.Ht

## I. INTRODUCTION

Directed (or oriented) percolation (DP) is a fundamental model in non-equilibrium statistical mechanics. A variety of natural phenomena can be modeled by DP, including forest fires [1, 2], epidemic diseases [3], and transport in porous media [4, 5].

A major reason for the longstanding interest in DP is its conjectured universality, first described by Janssen [6] and Grassberger [7]. Specifically, it is believed that any model possessing the following properties will belong to the DP universality class: short-range interactions; a continuous phase transition into a unique absorbing state; a one-component order parameter and no additional symmetries.

At and above the upper critical dimension ( $d_c = 4$ ), mean-field values for the critical exponents  $\beta = 1$ ,  $\nu_{\parallel} = 1$ ,  $\nu_{\perp} = 1/2$  are believed to hold. For  $d < d_c$  however, no exact results for either critical exponents or thresholds are known, and instead one relies on numerical estimates obtained by series analysis, transfer matrix methods, and Monte Carlo simulations. In  $(1+1)$  dimensions, series analysis [8, 9] has enabled the threshold estimates on several lattices to be determined to the eighth decimal place, with the critical exponents being estimated to the sixth decimal place.

Estimates of thresholds and critical exponents for  $d \geq 2$  can be found in [10–16]. Compared with results for  $d = 1$  however, the precision of these estimates in higher dimensions is less satisfactory. The central undertaking of the present work is to use high-precision Monte Carlo simulations to systematically study the thresholds of bond and site DP on simple-cubic (SC) and body-centered-cubic (BCC) lattices for  $2 \leq d \leq 7$ .

In order to obtain precise estimates of the critical thresholds, we study the finite-size scaling of the dimen-

sionless ratio  $Q_t = N_{2t}/N_t$ , where  $N_t$  is the mean number of sites becoming wet at time  $t$ .

Having obtained these estimates for  $p_c$ , we then fix  $p$  to our best estimate of  $p_c$  and use finite-size scaling to obtain improved estimates of the critical exponents for  $d = 2, 3$ . In addition, we also study the finite-size scaling at  $p_c$  of the distribution

$$p_{\mathcal{N}}(t, s) := \mathbb{P}(\mathcal{N}_t = s | \mathcal{N}_t > 0), \quad (1)$$

where  $\mathcal{N}_t$  is the number of sites becoming wet at time  $t$ . We conjecture, and numerically confirm, that

$$p_{\mathcal{N}}(t, s) \sim t^{-y_{\mathcal{N}}} F_{\mathcal{N}}(s/t^{y_{\mathcal{N}}}), \quad t \rightarrow \infty, \quad (2)$$

with exponent  $y_{\mathcal{N}} = \theta + \delta$ , where  $\theta = (d\nu_{\perp} - \beta)/\nu_{\parallel}$  and  $\delta = \beta/\nu_{\parallel}$  for  $d < d_c$  and  $y_{\mathcal{N}} = 1$  for  $d \geq d_c$ . We also study an analogous distribution of the random radius of gyration, as in Eq. (2) with  $y_{\mathcal{N}}$  being replaced by  $y_{\mathcal{R}} = \nu_{\perp}/\nu_{\parallel}$ .

The remainder of this paper is organized as follows. Section II introduces the DP models we study and describes how the simulations were performed. Results are presented in Secs. III, IV and V. We conclude with a discussion in Sec. VI. In Appendix A we present estimated thresholds of bond and site DP on the square, triangle, honeycomb and kagome lattices, while Appendix B contains some technical results justifying the definitions of the improved estimators defined in Sec. IID.

## II. DESCRIPTION OF THE MODEL AND SIMULATIONS

### A. Generating DP configurations

Although DP was originally introduced from a stochastic-geometric perspective [1], as the natural analog of isotropic percolation to oriented lattices, the most common formulation of DP is as a stochastic cellular automaton. To obtain a stochastic formulation of DP on a given oriented lattice, one defines a sequence  $(V_t)_{t \geq 0}$

\* tim.garoni@monash.edu

† yjdeng@ustc.edu.cn

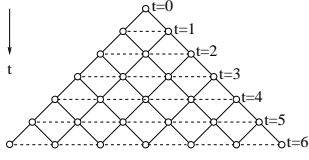


FIG. 1. Stochastic formulation of DP on the square lattice. The vertical direction corresponds to time, and the dashed lines identify the sets  $V_t$ .

which partitions the set of lattice sites, such that each adjacent site directed to  $v \in V_t$  belongs to some  $V_{t'}$  with  $t' < t$ . See Fig. 1 for the example of the square lattice. By setting  $V_0 = \{0\}$ , the trajectory of the stochastic process then generates the cluster connected to the origin. Typically  $t' = t - 1$ , and the resulting process is then Markovian.

For both site and bond DP, at time  $t$  the stochastic process visits each site  $v \in V_t$  and sets either  $s_v = 1$  (wet) or  $s_v = 0$  (dry). In more detail, the process proceeds as follows. At  $t = 0$ , we wet the origin with probability 1. At time  $t > 0$ , we construct for each  $v \in V_t$  the (random) set  $E_v$  of edges directed from wet sites to  $v$ . In the case of site DP, if  $E_v$  is non-empty we set  $s_v = 1$  with probability  $p$ , otherwise we set  $s_v = 0$ . For bond DP, we select an edge  $e \in E_v$  and occupy it with probability  $p$ . If  $e$  is occupied, we set  $s_v = 1$ , and then proceed to update the next site in  $V_t$ . If  $e$  is unoccupied, we repeat the procedure for the next edge in  $E_v$ , and continue until either an edge is occupied or the set  $E_v$  is exhausted [17].

We note that in this description, the sets  $V_t$  have been given a pre-specified order, as have the sets of edges incident to each  $v \in V_t$ . The precise form of these orderings is obviously unimportant, and in practice they were induced in the natural way from the coordinates of the vertices. We used a hash table [18] to store the wet sites in our simulations, as described in [19].

For  $p > p_c$ , there is a non-zero probability that the number of wet sites will diverge as  $t \rightarrow \infty$ . In our simulations, the cluster growth stops either at the first time that no new sites become wet, or when  $t = t_{\max}$ , where  $t_{\max}$  is predetermined. The values of  $t_{\max}$  used for each simulation were chosen as follows. For site and bond DP with  $2 \leq d \leq 5$ , we set  $t_{\max} = 2^{14}$ . On SC lattice with  $d = 6, 7$ , we set  $t_{\max} = 2^{13}$  and  $t_{\max} = 2^{11}$  respectively. On BCC lattice with  $d = 6, 7$ , we set  $t_{\max} = 2^{12}$  and  $t_{\max} = 2^{10}$  respectively. In all cases, the number of independent samples generated was  $10^9$ .

## B. Lattices

We simulated  $(d + 1)$ -dimensional simple-cubic (SC) and body-centered cubic (BCC) lattices with  $2 \leq d \leq 7$ . The stochastic processes formulation of DP on these lattices that we used in our simulations is Markovian, and is described most easily by explicitly describing the

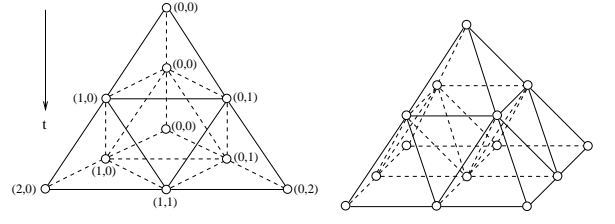


FIG. 2. (2+1)-dimensional SC (left) and BCC (right) lattices.

sets  $V_t$  together with the edges between  $V_t$  and  $V_{t+1}$ . In  $(d + 1)$  dimensions, each  $V_t \subset \mathbb{Z}^d$ . Let  $\mathbf{x} \in V_t$ , and let  $\{\mathbf{e}_1, \dots, \mathbf{e}_d\}$  denote the standard basis of  $\mathbb{Z}^d$ . On the BCC lattice, the coordinates of the  $\lambda = 2^d$  neighbors of  $\mathbf{x}$  in  $V_{t+1}$  are  $\mathbf{x} + \sum_{i=1}^d \alpha_i \mathbf{e}_i$  for  $\alpha \in \{0, 1\}^d$ . On the SC lattice, the coordinates of the  $\lambda = d + 1$  neighbors of  $\mathbf{x}$  in  $V_{t+1}$  are  $\mathbf{x} + \sum_{i=1}^d \alpha_i \mathbf{e}_i$  for all  $\alpha \in \{0, 1\}^d$  with  $\|\alpha\|_1 \leq 1$ . The (2+1)-dimensional cases are illustrated in Fig. 2.

## C. Observables

For each simulation we sampled the following random variables:

1.  $\mathcal{N}_t$ , the number of sites becoming wet at time  $t$ ;
2.  $\mathcal{S}_t = \sqrt{\sum_v r_v^2}$ , where  $r_v$  denotes the Euclidean distance of the site  $v$  to the time axis, and the sum is over all wet sites in  $V_t$ ;
3.  $\mathfrak{N}_t = \sum_{v \in V_t} b_v$ , where  $b_v$  is the number of Bernoulli trials needed to determine the state of  $v \in V_t$ , given the configuration of sites in  $V_{t-1}$ ;
4.  $\mathfrak{S}_t = \sqrt{\sum_{v \in V_t} b_v r_v^2}$ .

We note that, as shown in Appendix B, we have

$$\langle \mathcal{N}_t \rangle = p \langle \mathfrak{N}_t \rangle, \quad (3)$$

$$\langle \mathcal{S}_t^2 \rangle = p \langle \mathfrak{S}_t^2 \rangle, \quad (4)$$

where  $\langle \cdot \rangle$  denotes the ensemble average. As explained in Section II D,  $\mathfrak{N}_t$  and  $\mathfrak{S}_t$  can be used to construct reduced-variance estimators.

Using the above random variables, we then estimated the following quantities:

1. The percolation probability  $P_t = \mathbb{P}(\mathcal{N}_t > 0)$ ;
2. The mean number of sites becoming wet at time  $t$ ,  $N_t = \langle \mathcal{N}_t \rangle$ ;
3. The dimensionless ratio  $Q_t = N_{2t}/N_t$ ;
4. The radius of gyration  $R_t^2 = \langle \mathcal{S}_t^2 \rangle / N_t$ ;
5. The distribution  $p_{\mathcal{N}}(t, s)$  defined by (1);

## 6. The distribution

$$p_{\mathcal{R}}(t, s) := \mathbb{P}(\mathcal{R}_t = s | \mathcal{N}_t > 0) \quad (5)$$

where

$$\mathcal{R}_t := \begin{cases} \frac{\mathcal{S}_t}{\sqrt{\mathcal{N}_t}}, & \mathcal{N}_t > 0, \\ 0, & \mathcal{N}_t = 0. \end{cases} \quad (6)$$

We expect the second moment of  $p_{\mathcal{R}}(t, \cdot)$  to display the same critical scaling as the radius of gyration. We discuss this point further in Sec. V.

## D. Improved Estimators

To estimate  $N_t$ ,  $R_t^2$  and  $Q_t$ , we adopted the variance reduction technique introduced in [16, 19, 20], the details of which we now describe. To clearly distinguish sample means generated by our simulated data from the ensemble averages to which they converge, we will use  $\bar{X} = \sum_{i=1}^n X^{(i)}/n$  to denote the sample mean of  $n$  independent realizations  $X^{(1)}, \dots, X^{(n)}$  of the random variable  $X$ . While  $\lim_{n \rightarrow \infty} \bar{X} = \langle X \rangle$ , we emphasize that  $\bar{X}$  is a random variable for any finite  $n$ .

In addition to the naive estimator  $\bar{\mathcal{N}}_t$ , we can also estimate  $N_t$  via

$$\widehat{N}_t := p^t \prod_{t'=1}^t \frac{\bar{\mathfrak{N}}_{t'}}{\bar{\mathcal{N}}_{t'-1}}. \quad (7)$$

Indeed, taking the number of samples to infinity and using (3) we find

$$\widehat{N}_t = p^t \prod_{t'=1}^t \frac{\bar{\mathfrak{N}}_{t'}}{\bar{\mathcal{N}}_{t'-1}} \rightarrow \prod_{t'=1}^t \frac{N_{t'}}{N_{t'-1}} = N_t. \quad (8)$$

Any convex combination of  $\bar{\mathcal{N}}_t$  and the estimator (7) will therefore also be an estimator for  $N_t$ . As our final estimator for  $N_t$  we therefore used

$$\alpha \bar{\mathcal{N}}_t + (1 - \alpha) \widehat{N}_t, \quad (9)$$

with  $\alpha = \alpha_{\min}$  chosen so as to minimize the variance of (9). Explicitly,

$$\alpha_{\min} = \frac{\text{var}(\widehat{N}_t) - \text{cov}(\bar{\mathcal{N}}_t, \widehat{N}_t)}{\text{var}(\bar{\mathcal{N}}_t) + \text{var}(\widehat{N}_t) - 2\text{cov}(\bar{\mathcal{N}}_t, \widehat{N}_t)}. \quad (10)$$

Note that  $\alpha_{\min}$  can be readily estimated from the simulation data. Similarly, to estimate  $Q_t$  we use the minimum-variance convex combination of  $\bar{\mathcal{N}}_{2t}/\bar{\mathcal{N}}_t$  and  $\widehat{N}_{2t}/\widehat{N}_t$ .

An analogous estimator for  $R_t^2$  can also be constructed:

$$\widehat{R}_t^2 = \sum_{t'=1}^t \left( \frac{\bar{\mathfrak{S}}_{t'}^2}{\bar{\mathfrak{N}}_{t'}} - \frac{\bar{\mathcal{S}}_{t'-1}^2}{\bar{\mathcal{N}}_{t'-1}} \right), \quad (11)$$

Taking the number of samples to infinity and using (4) shows that indeed  $\widehat{R}_t^2 \rightarrow R_t^2$ . Analogously to the argument above, we then take the convex combination of  $\widehat{R}_t^2$  and  $\bar{\mathcal{S}}_t^2/\bar{\mathcal{N}}_t$  with minimum variance to be our final estimator for  $R_t^2$ .

We now comment on the motivation behind these definitions. For DP on a  $\lambda$ -ary tree we have the simple identity  $\mathfrak{N}_t = \lambda \mathcal{N}_{t-1}$ , which implies that  $\widehat{N}_t$  is deterministic in this case, and therefore has precisely zero variance. For DP on a  $(d+1)$ -dimensional lattice, as  $d$  increases the updates become more and more like the updates for DP on the  $\lambda$ -ary tree, and so intuitively one expects that the variance of  $\widehat{N}_t$  should decrease as  $d$  increases. This is indeed what we observe numerically. For the simulations of bond DP on the BCC lattice for example, we find that for  $d = 4$  the variance of  $\widehat{N}_t$  is  $\approx 0.1$  of the variance of  $\bar{\mathcal{N}}_t$ . This factor reduces to  $10^{-4}$  for  $d = 7$ . For low dimensions, however, the above variance reduction technique is less effective. Similar arguments and observations apply to the reduced-variance estimator for the radius of gyration. Interestingly, our data suggest that the above technique is more effective for bond DP than site DP.

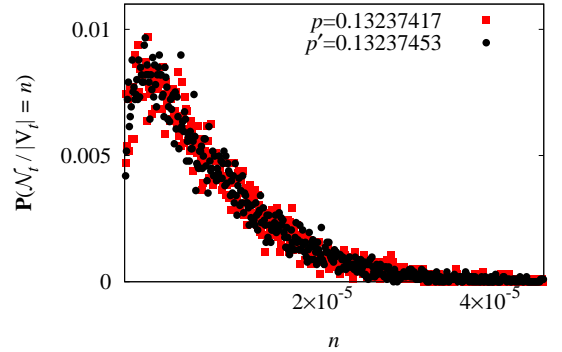


FIG. 3. (Color online) Plot of  $\mathbb{P}(\mathcal{N}_t/|V_t| = \cdot)$  at  $t = 16384$  for  $d = 3$  bond DP on BCC lattice, with  $p = 0.13237417$  (square) and  $p' = 0.13237453$  (circle).

## III. PERCOLATION THRESHOLDS

### A. Fitting Methodology

To estimate the critical threshold  $p_c$  we applied an iterative approach. We ran preliminary simulations at several values of  $p$  and relatively small values of  $t_{\max}$ , and used these data to estimate  $p_c$  by studying the finite-size scaling of  $Q_t$ . Further simulations were then performed at and near the value of  $p_c$  estimated in the initial runs, using somewhat larger values of  $t_{\max}$ . For both site and bond DP, and for each choice of lattice and dimension, this procedure was iterated a number of times before we

	$p_c$	$Q_c$	$y_{  }$	$q_1$	$q_2$	$c_1$	$y_u$	$t_{\min}/\text{DF}/\chi^2$
$\text{SC}_2^b$	0.382 224 62(2)	1.173 42(4)	0.776 7(4)	-3.127(7)	2.25(3)	-0.011(1)	-0.5	64/224/175
$\text{SC}_2^s$	0.435 314 10(5)	1.173 42(2)	0.777 4(3)	-2.403(5)	1.37(2)	-0.025(6)	-0.48(7)	64/223/168
$\text{BCC}_2^b$	0.287 338 37(2)	1.173 36(2)	0.776 2(4)	-4.177(9)	4.26(4)	-6(3)	-2.1(2)	64/224/235
$\text{BCC}_2^s$	0.344 574 01(4)	1.173 41(2)	0.777 2(3)	-2.879(6)	1.95(2)	-0.31(2)	-0.54(7)	64/223/82
$\text{SC}_3^b$	0.268 356 28(1)	1.076 52(8)	0.905(4)	-3.8(2)	5.6(3)	0.005(1)	-0.3	64/223/166
$\text{SC}_3^s$	0.303 395 39(2)	1.075 2(4)	0.906(4)	-2.7(1)	2.9(2)	0.024(1)	-0.26(2)	64/223/367
$\text{BCC}_3^b$	0.132 374 169(3)	1.076 29(6)	0.904(2)	-8.5(2)	28.6(9)	-0.032(3)	-0.62(3)	64/359/341
$\text{BCC}_3^s$	0.160 961 28(1)	1.076 7(3)	0.904(4)	-5.0(2)	10.0(6)	0.026(1)	-0.34(2)	64/223/163

TABLE I. Fit results for  $Q_t$  with  $d = 2, 3$  on the SC and BCC lattices. Superscripts  $b$  and  $s$  represent bond and site DP, respectively. The subscript represents the dimensionality  $d$ .

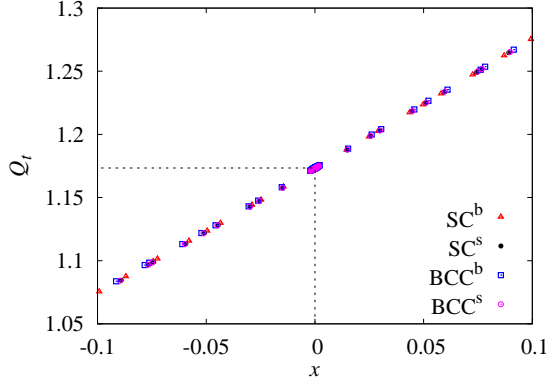


FIG. 4. (Color online) Plot of the  $Q_t$  data for bond and site DP on the SC and BCC lattices versus  $x = q_1(p_c - p)t^{y_{||}}$  for  $d = 2$ .

	$p_c$	$q_1$	$c_1$	$h_1$	$t_{\min}$
$\text{SC}_4^b$	0.207 918 153(3)	-5.2(9)	-0.22(2)	0.50(2)	64
$\text{SC}_4^s$	0.231 046 861(3)	-3.83(1)	-0.53(2)	-1.2(1)	64
$\text{BCC}_4^b$	0.063 763 395(1)	-18.6(1)	-0.08(1)	3.34(3)	64
$\text{BCC}_4^s$	0.075 585 154(2)	-11.4(4)	-0.55(2)	-1.12(2)	64

TABLE II. Fit results for  $Q_t$  with  $d = 4$  on the SC and BCC lattices. Superscripts  $b$  and  $s$  represent bond and site DP, respectively. The subscript represents the dimensionality  $d$ .

performed our final high-precision runs at the single value of  $p$  which corresponded to the best estimate of  $p_c$  obtained in the preliminary simulations. For these final simulations we used the values of  $t_{\max}$  reported in Section II A.

For computational efficiency, we then used re-weighting to obtain expectations corresponding to multiple values of  $p$ , from each of our final high-precision runs. Our approach to re-weighting is similar to that described for the contact process in [21], and relies on the simple observation that for any observable  $\mathcal{A}_t$  we have the identity  $\langle \mathcal{A}_t \rangle_{p'} = \langle \mathcal{W}_{p,p'} \mathcal{A}_t \rangle_p$ , where the random variable

$\mathcal{W}_{p,p'}$  is defined on the space of site configurations  $C$  by

$$\mathcal{W}_{p,p'}(C) = \frac{\mathbb{P}_{p'}(C)}{\mathbb{P}_p(C)} = \prod_{t=1}^{t_{\max}} \left( \frac{p'}{p} \right)^{\mathcal{N}_t(C)} \left( \frac{1-p'}{1-p} \right)^{\mathfrak{N}_t(C) - \mathcal{N}_t(C)}.$$

As with any application of re-weighting, in practice one must of course be careful that the distributions  $\mathbb{P}_p(\cdot)$  and  $\mathbb{P}_{p'}(\cdot)$  have sufficient overlap, so that a finite simulation with parameter  $p$  will generate sufficiently many samples in the neighbourhood of the peak of  $\mathbb{P}_{p'}(\cdot)$ . As  $t$  increases, the range of acceptable  $p'$  values is expected to decrease. To verify that we had sufficient overlap, for both bond and site DP and for each choice of lattice and dimension, we performed additional low-statistics simulations ( $10^7$  independent samples, rather than  $10^9$ ) for the  $p'$  values furthest from  $p$ , and compared the histograms generated at  $t = t_{\max}$  for simulations at  $p'$  with those generated at  $p$ . In all cases the overlap was excellent. Figure 3 gives a typical example, showing the estimated distribution  $\mathbb{P}(\mathcal{N}_t/|V_t| = \cdot)$  at  $t = 16384$  for  $d = 3$  bond DP on the BCC lattice, with  $p = 0.132\,374\,17$  and  $p' = 0.132\,374\,53$ .

These final high-precision data sets were then used to perform our final fits for  $p_c$ , which we report in Tables I, II and III. Specifically, we performed least-squares fits of the  $Q_t$  data to an appropriate finite-size scaling ansatz. As a precaution against correction-to-scaling terms that we failed to include in the chosen ansatz, we imposed a lower cutoff  $t > t_{\min}$  on the data points admitted in the fit, and we systematically studied the effect on the  $\chi^2$  value of increasing  $t_{\min}$ . In general, our preferred fit for any given ansatz corresponds to the smallest  $t_{\min}$  for which the goodness of fit is reasonable and for which subsequent increases in  $t_{\min}$  do not cause the  $\chi^2$  value to drop by vastly more than one unit per degree of freedom. In practice, by “reasonable” we mean that  $\chi^2/\text{DF} \lesssim 1$ , where DF is the number of degrees of freedom.

In Table I, II and III, we list the results for our preferred fits for  $Q_t$ , with  $d$  from 2 to 7. The superscripts “b” and “s” are used in these tables to distinguish the bond and site DP, and the subscript denotes the dimensionality  $d$ . The error bars reported in Tables I, II and III correspond to statistical error only. To estimate the systematic error in our estimates of  $p_c$  we studied the robustness of the fits to variations in the terms retained in

	$p_c$	$q_1$	$q_2$	$c$	$c_1$	$y_u$	$t_{\min}/\text{DF}/\chi^2$
$\text{SC}_5^b$	0.170 615 153(1)	-5.253(5)	13.5(2)	-0.72(7)	0.026(1)	-0.49(1)	48/258/208
$\text{SC}_5^s$	0.186 513 581(2)	-4.115(6)	8.6(1)	-1.17(9)	0.054(1)	-0.49(1)	48/258/172
$\text{BCC}_5^b$	0.031 456 631 6(1)	-30.78(4)	450(6)	-1.6(7)	0.009(1)	-0.48(1)	48/248/176
$\text{BCC}_5^s$	0.035 972 542 1(5)	-21.17(5)	164(7)	-5.3(7)	0.049(1)	-0.48(1)	48/242/119
$\text{SC}_6^b$	0.145 089 946 5(4)	-6.538(2)	21.4(2)	-	0.028(1)	-0.99(1)	48/235/147
$\text{SC}_6^s$	0.156 547 177(3)	-5.428(4)	13.1(4)	-	0.051(3)	-0.87(2)	64/193/55
$\text{BCC}_6^b$	0.015 659 382 96(3)	-63.394(8)	1945(30)	-	0.003(1)	-0.99(3)	48/193/110
$\text{BCC}_6^s$	0.017 333 051 7(4)	-49.33(4)	1343(27)	-	0.043(1)	-0.88(2)	48/198/79
$\text{SC}_7^b$	0.126 387 509 0(6)	-7.663(2)	28.9(4)	-	0.015(2)	-1.32(3)	32/225/196
$\text{SC}_7^s$	0.135 004 173(2)	-6.566(4)	20.8(5)	-	0.092(6)	-1.45(2)	32/225/212
$\text{BCC}_7^b$	0.007 818 371 82(1)	-127.63(1)	7557(157)	-	0.0007(2)	-1.31(8)	32/176/171
$\text{BCC}_7^s$	0.008 432 989 5(3)	-107.0(2)	3882(1000)	-	0.036(5)	-1.29(4)	32/181/84

TABLE III. Fit results for  $Q_t$  with  $d = 5, 6, 7$  on the SC and BCC lattices. Superscripts  $b$  and  $s$  represent bond and site DP, respectively. The subscript represents the dimensionality  $d$ .

the fitting ansatz and in  $t_{\min}$ . This produced the final estimates of the critical thresholds shown in Table IV.

### B. Results for $d = 2, 3$

Near the critical point  $p_c$ , we expect that

$$Q_t(p) = \tilde{Q}(vt^{y_{\parallel}}, ut^{y_u}), \quad (12)$$

where  $v$  and  $u$  represent the amplitudes of the relevant and the leading irrelevant scaling fields, respectively, and  $y_{\parallel} = 1/\nu_{\parallel}$  and  $y_u < 0$  are the associated renormalization exponents. Linearizing  $v \approx a_1(p_c - p)$  around  $p = p_c$  we can expand  $Q_t$  as

$$Q_t = Q_c + \sum_{k \geq 1} q_k (p_c - p)^k t^{ky_{\parallel}} + c(p_c - p)t^{y_{\parallel} + y_u} + c_1 t^{y_u} + \dots \quad (13)$$

where  $Q_c = 2^{\theta}$  and  $q_k = a_1^k \frac{\partial^k \tilde{Q}}{\partial v^k}|_{v=0}$ . It follows that  $q_k/(q_1)^k$  is a universal quantity. In practice, we neglected terms higher than cubic in the finite-size scaling variable  $(p_c - p)t^{y_{\parallel}}$ .

We fitted our data for  $Q_t$  to the ansatz (13) as described above, and the results are reported in Table I. From the fits for site DP, we observe that on both the SC and BCC lattices, the leading correction exponent  $y_u \approx -0.5$  for  $d = 2$ , and  $y_u \approx -0.3$  for  $d = 3$ . However, for bond DP on the BCC lattice, the fits yield  $y_u \approx -2$  for  $d = 2$ , and  $y_u \approx -0.6$  for  $d = 3$ . This suggests that, within the resolution of our simulations, the amplitude  $c_1$  is consistent with zero in this case. For the fits for bond DP on the SC lattice, we could not obtain numerically stable fits with  $y_u$  left free, and so we instead report the results using correction terms  $c_1 t^{-0.5} + c_2 t^{-2}$  for  $d = 2$  and  $c_1 t^{-0.3} + c_2 t^{-2}$  for  $d = 3$ .

For  $d = 2$ , we estimate  $Q_c = 1.173\,40(6)$ ,  $\nu_{\parallel} = 1/y_{\parallel} = 1.287(2)$ , and  $q_2/q_1^2 = 0.24(1)$ . For  $d = 3$ , we estimate  $Q_c = 1.076(1)$ ,  $\nu_{\parallel} = 1/y_{\parallel} = 1.104(6)$ , and  $q_2/q_1^2 = 0.40(1)$ .

In Fig. 4 we plot the  $Q_t$  data versus  $q_1(p_c - p)t^{y_{\parallel}}$ , for bond and site DP on the two-dimensional SC and BCC lattices. We use the estimated value  $y_{\parallel} \approx 0.777$ , and  $q_1$  and  $p_c$  are taken respectively from Table I and Table IV. An excellent collapse is observed in Fig. 4. The data for  $t < 1024$  have been excluded to suppress the effects of finite-size corrections. The data collapse to a line with slope 1 clearly demonstrates universality.

### C. Results for $d = 4$

At the upper critical dimension, the existence of dangerous irrelevant scaling fields typically leads to both multiplicative and additive logarithmic corrections to the mean-field behavior. Field-theoretic arguments [22, 23] predict that in the neighborhood of criticality

$$N_t \sim \left( \ln \frac{t}{t_0} \right)^{\alpha} \Phi \left( (p_c - p)t^{y_{\parallel}} \left( \ln \frac{t}{t_2} \right)^{-\alpha}, ut^{y_u} \right), \quad (14)$$

with  $\alpha = 1/6$ ,  $y_{\parallel} = 1$  and  $\Phi$  a universal scaling function. From (14) we then obtain

$$Q_t = \left( 1 + \frac{\ln 2}{\ln t + h_1} \right)^{1/6} + c(p_c - p) \frac{t^{1+y_u}}{(\ln t + h_2)^{1/6}} + \sum_{k \geq 1} q_k (p_c - p)^k \frac{t^k}{(\ln t + h_2)^{k/6}} + c_1 t^{y_u} + \dots \quad (15)$$

We fitted the  $d = 4$  data for  $Q_t$  to the ansatz (15), and the results of our preferred fits are reported in Table II. In the reported fits, we fixed  $c = 0$  and  $h_2 = 0$  since performing fits with them left free produced estimates for both which were consistent with zero. We could not obtain stable fits with  $y_u$  left free, and so the reported fits use  $y_u = -1$ ; the resulting estimate of  $p_c$  was robust against variations in the fixed value of  $y_u$ . All  $q_i$  with  $i \geq 3$  were set identically to zero. In addition, to suppress the effects of various higher-order corrections associated with the deviation  $|p_c - p|$ , we only fitted the  $Q_t$  data



Lattice	Site		Bond	
	$p_c(\text{Present})$	$p_c(\text{Previous})$	$p_c(\text{Present})$	$p_c(\text{Previous})$
$d = 2, \text{SC}$	0.435 314 11(10)	0.435 31(7) [10]	0.382 224 62(6)	0.382 223(7) [10]
$d = 2, \text{BCC}$	0.344 574 0(2)	0.344 573 6(3) [11] 0.344 575(15) [13]	0.287 338 38(4)	0.287 338 3(1) [12] 0.287 338(3) [10]
$d = 3, \text{SC}$	0.303 395 38(5)	0.302 5(10) [14]	0.268 356 28(5)	0.268 2(2) [15]
$d = 3, \text{BCC}$	0.160 961 28(3)	0.160 950(30) [13]	0.132 374 17(2)	-
$d = 4, \text{SC}$	0.231 046 86(3)	-	0.207 918 16(2)	0.208 5(2) [15]
$d = 4, \text{BCC}$	0.075 585 15(1)	0.075 585 0(3) [16] 0.075 582(17) [13]	0.063 763 395(5)	-
$d = 5, \text{SC}$	0.186 513 58(2)	-	0.170 615 155(5)	0.171 4(1) [15]
$d = 5, \text{BCC}$	0.035 972 540(3)	0.035 967(23) [13]	0.031 456 631 8(5)	-
$d = 6, \text{SC}$	0.156 547 18(1)	-	0.145 089 946(3)	0.145 8 [15]
$d = 6, \text{BCC}$	0.017 333 051(2)	-	0.015 659 382 96(10)	-
$d = 7, \text{SC}$	0.135 004 176(10)	-	0.126 387 509(3)	0.127 0(1) [15]
$d = 7, \text{BCC}$	0.008 432 989(2)	-	0.007 818 371 82(6)	-

TABLE IV. Final estimates of critical thresholds for bond and site DP on the SC and BCC lattices, with  $2 \leq d \leq 7$ . A dash “-” implies that we are unaware of any previous estimates in the literature.

corresponding to  $p$  values which were sufficiently close to  $p_c$  that  $q_2$  was consistent with zero. Thus, in Table II, we do not report estimates for  $q_2$ .

#### D. Result for $d = 5, 6, 7$

For  $d > d_c$ , we fitted the data for  $Q_t$  to the ansatz (13) with  $Q_c$  and  $y_{\parallel}$  fixed at their mean-field values [24],  $Q_c = 1 = y_{\parallel}$ . The results are reported in Table III. Repeating the fits with  $Q_c$  and  $y_{\parallel}$  left free produced estimates in perfect agreement with the predicted values. For  $d = 6$  and 7, leaving the amplitude  $c$  free produced estimates consistent with zero, and we therefore omitted this term in the reported fits.

From Table III, we observe that the universal amplitude  $q_2/q_1^2 \approx 0.5$  holds for all models in  $d = 5, 6$  and 7 dimensions. We also observe that the leading correction exponents  $y_u$  are  $\approx -1/2, -1, -3/2$  for  $d = 5, 6$ , and 7, respectively, in agreement with the field-theoretic prediction [22] of  $y_u = 2 - d/2$ .

#### E. Summary of thresholds

We summarize our final estimates of the critical thresholds for  $2 \leq d \leq 7$  in Table IV. The error bars in these final estimates of  $p_c$  are obtained by estimating the systematic error from a comparison of the results from a number of different fits, varying both the terms retained in the fitting ansatz and the value of  $t_{\min}$  used. For comparison, we also present several previous estimates from the literature.

To illustrate the accuracy of our threshold estimates, we plot in Fig. 5 the data for  $Q_t$  versus  $t$  for a number of DP models. At the critical point, the data for  $Q_t$  should tend to a horizontal line as  $t$  increases, while the data with  $p \neq p_c$  will bend upwards or downwards. In each case in Fig. 5, the central curve corresponds to our

estimated  $p_c$ , and the other two curves correspond to the  $p$  values which are the estimated  $p_c$  plus or minus three error bars.

We conclude this section with some observations regarding the  $p_c$  values reported in Table IV. Based on empirical observations, [25] conjectured the ansatz

$$1/p_c \approx a_1 + a_2 \lambda, \quad \text{for } \lambda \gg 1, \quad (16)$$

relating  $p_c$  to the coordination number  $\lambda$ , when  $\lambda$  is large. In Fig. 6, we plot  $1/p_c$  versus  $\lambda$ . We observe that on the SC lattice, the slopes for bond and site DP are approximately equal, while on the BCC lattice the bond and site cases clearly differ. In Table V we report the values of  $a_1$  and  $a_2$  obtained by fitting (16) to the  $d \geq 4$  data for  $p_c$  from Table IV. From Table V we conjecture that  $a_2$  is identical for bond and site DP on the SC lattice.

	SC <sup>b</sup>	SC <sup>s</sup>	BCC <sup>b</sup>	BCC <sup>s</sup>
$a_1$	-0.35(4)	-0.71(2)	-0.23(4)	-2.6(4)
$a_2$	1.034(5)	1.026(2)	1.0011(4)	0.946(5)

TABLE V. Estimates of  $a_1$  and  $a_2$  in (16), calculated from the  $d \geq 4$  data.

$\mathcal{O}(t)$	$y_{\mathcal{O}}$	$c_0$	$c_1$	$c_2$	$t_{\min}$
$N_t$	0.230 70(7)	0.976 0(5)	0.004(4)	4(2)	64
$P_t$	-0.451 1(2)	0.830 6(8)	0.83(9)	-30(5)	96
$R_t^2$	1.132 19(4)	1.633 7(5)	1.09(4)	-4(2)	64
$\bar{N}_t$	0.105 58(10)	0.958 2(7)	0.33(5)	-4(2)	64
$\bar{P}_t$	-0.740 3(3)	1.069(3)	0.6(3)	-60(12)	64
$\bar{R}_t^2$	1.053 01(7)	2.715(2)	2.2(2)	-60(15)	128

TABLE VI. Fits results of  $N_t$ ,  $P_t$ , and  $R_t^2$  on the BCC lattice for  $d = 2$  (top) and 3 (bottom). The leading correction exponent  $y_u$  was fixed to  $-1$ .

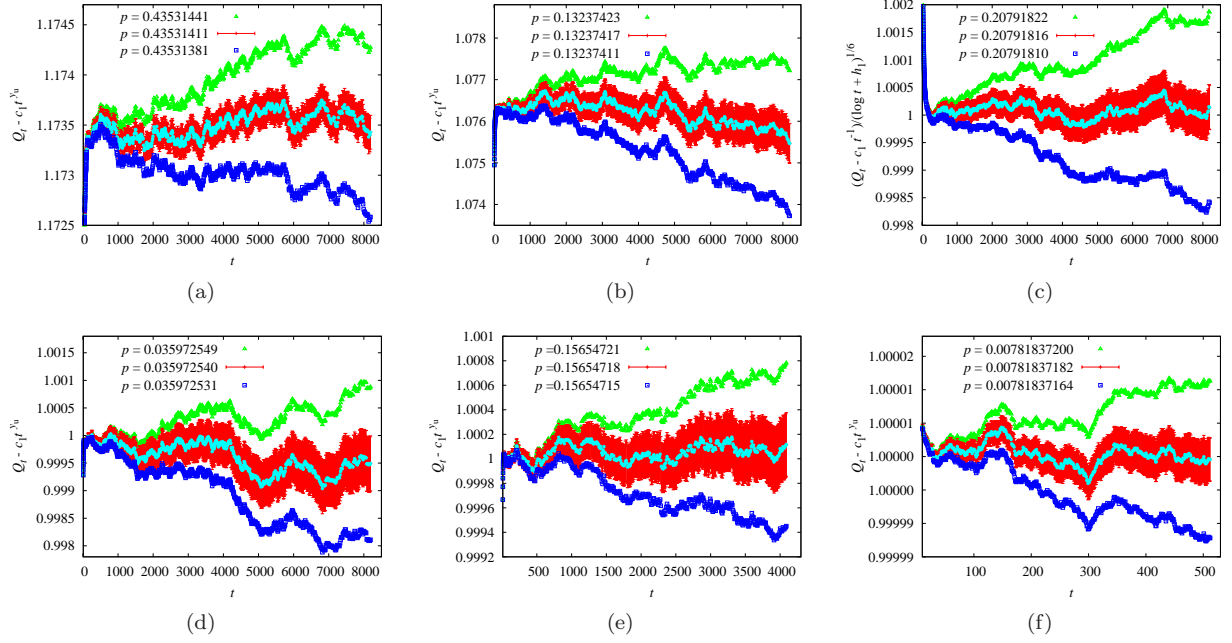


FIG. 5. (Color online) Plots of  $Q_t - c_1 t^{y_u}$  (for  $d \neq 4$ ) and  $(Q_t - c_1 t^{-1})/(\log t + h_1)^{1/6}$  (for  $d = 4$ ) versus  $t$  for several DP models. The subfigures (a) to (f) respectively correspond to  $d = 2$  SC site DP,  $d = 3$  BCC bond DP,  $d = 4$  SC bond DP,  $d = 5$  BCC site DP,  $d = 6$  SC site DP and  $d = 7$  BCC bond DP. The values of  $c_1$ ,  $y_u$  and  $h_1$  are our best estimates, taken from Tables I, II and III. The three curves show the Monte Carlo data corresponding to the central value of our estimated  $p_c$ , and the central value of  $p_c$  plus or minus three error bars (from Table IV). The curve corresponding to  $p_c$  is plotted with its statistical error, corresponding to one standard error.

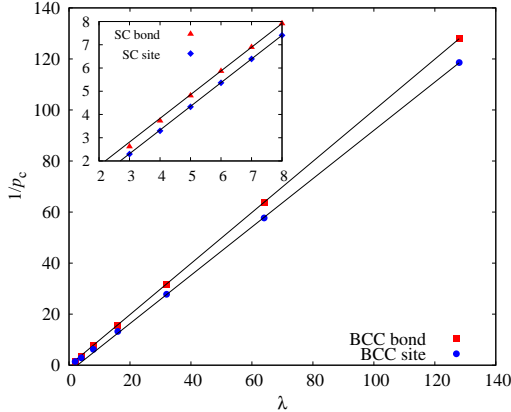


FIG. 6. (Color online) Plot of  $1/p_c$  versus coordination number  $\lambda$  for bond and site DP on the BCC lattice. The lines are obtained by fitting (16) to the  $d \geq 4$  data. The inset shows the analogous plot for the SC lattice.

#### IV. CRITICAL EXPONENTS

At  $p = p_c$ , one expects

$$P_t \sim t^{-\delta}, \quad N_t \sim t^\theta, \quad R_t^2 \sim t^{2/z}. \quad (17)$$

The critical exponents  $\delta$ ,  $\theta$ ,  $z$  are related to the standard exponents  $\beta$ ,  $\nu_{\parallel}$ ,  $\nu_{\perp}$  by [24]

$$\delta = \beta/\nu_{\parallel}, \quad \theta = (d\nu_{\perp} - 2\beta)/\nu_{\parallel}, \quad \text{and} \quad z = \nu_{\parallel}/\nu_{\perp}. \quad (18)$$

Fixing  $p$  to our best estimate of  $p_c$  from Table IV, we estimated the critical exponents  $\theta$ ,  $\delta$ , and  $z$  for  $d = 2$  and 3, by studying the critical scaling of  $N_t$ ,  $P_t$  and  $R_t^2$ . Specifically, we fitted the data for  $N_t$ ,  $P_t$ , and  $R_t^2$  to the ansatz

$$\mathcal{O}(t) = t^{y_{\mathcal{O}}}(c_0 + c_1 t^{y_u} + c_2 t^{-2}), \quad (19)$$

where  $y_{\mathcal{O}}$  corresponds to  $\theta$ ,  $-\delta$  and  $2/z$ , respectively. We focused on the case of bond DP on the BCC lattice, since we find empirically that it suffers from the weakest corrections to scaling. In Table VI, we report the results of the fits with  $y_u$  fixed at  $-1$ . To estimate the systematic error in our exponent estimates we studied the robustness of the fits to variations in the fixed value of  $y_u$ , and in  $t_{\min}$ . This produced the final exponent estimates reported in Table VII.

For comparison, we also report in Table VII several previous exponent estimates from the literature. We note that our estimates of  $z$  and  $\theta$  in (3+1) dimensions are inconsistent with the field-theoretic predictions reported in [6, 26].

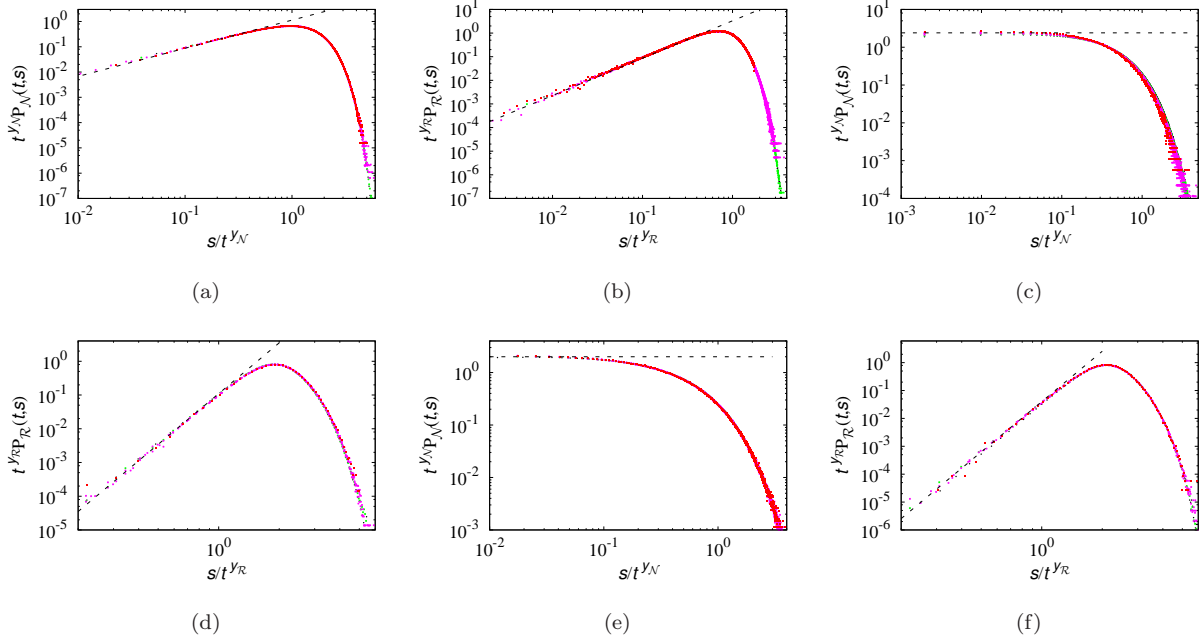


FIG. 7. (Color online) Log-log plots of  $t^{y_N} p_N(t, s)$  versus  $s/t^{y_N}$ , and  $t^{y_R} p_R(t, s)$  versus  $s/t^{y_R}$ . The subfigures (a) to (f) respectively correspond to  $p_N(t, s)$  for  $d = 1$ ,  $p_R(t, s)$  for  $d = 1$ ,  $p_N(t, s)$  for  $d = 4$ ,  $p_R(t, s)$  for  $d = 4$ ,  $p_N(t, s)$  for  $d = 5$  and  $p_R(t, s)$  for  $d = 5$ . The data correspond to bond DP on the square lattice ( $d = 1$ ) and BCC lattice ( $d = 4, 5$ ). The exponents  $y_N = \theta + \delta$  and  $y_R = 1/z$  are calculated from Table IX for  $d = 1$ , and are given by the exact mean-field values for  $d = 4$  and  $5$ . The dashed lines have slopes equal to  $1/y_N - 1$  and  $1/y_R - 1 + d$  for  $p_N(t, s)$  and  $p_R(t, s)$ , respectively.

$d$	Ref.	$\beta$	$\nu_{\parallel}$	$\nu_{\perp}$	$z$	$\theta$	$\delta$
2	Present	0.580(4)	1.287(2)	0.729(1)	1.7665(2)	0.2307(2)	0.4510(4)
	[10]		1.295(6)		1.765(3)	0.229(3)	0.451(3)
	[27]				1.766(2)	0.229 5(10)	0.450 5(10)
	[12]				1.766 6(10)	0.230 3(4)	0.450 9(5)
3	Present	0.818(4)	1.106(3)	0.582(2)	1.8990(4)	0.105 7(3)	0.739 8(10)
	[28]	0.813(11)	1.11(1)		1.901(5)	0.114(4)	0.732(4)
	[6]	0.822 05	1.105 71	0.583 60	1.887 46	0.120 84	0.737 17

TABLE VII. Final estimates of the critical exponents for  $d = 2$  and  $3$ .

## V. CRITICAL DISTRIBUTIONS

In this section we consider the critical scaling of  $p_N(t, s)$  and  $p_R(t, s)$ . From finite-size scaling theory, we expect that  $p_N(t, s)$  and  $p_R(t, s)$  should scale at criticality as

$$\begin{aligned} p_N(t, s) &\sim t^{-y_N} F_N(s/t^{y_N}), \\ p_R(t, s) &\sim t^{-y_R} F_R(s/t^{y_R}). \end{aligned} \quad (20)$$

The scaling functions  $F_N$  and  $F_R$  are expected to be universal. It follows immediately from (20) that for all  $k \in \mathbb{N}$  we have

$$\begin{aligned} \langle \mathcal{N}_t^k \rangle &\sim t^{k y_N - \delta}, \\ \langle \mathcal{R}_t^k \rangle &\sim t^{k y_R - \delta}. \end{aligned} \quad (21)$$

Since  $\langle \mathcal{N}_t \rangle \sim t^\theta$ , we can then identify

$$y_N = \theta + \delta. \quad (22)$$

Similarly, making the assumption that

$$\langle \mathcal{R}_t^2 \rangle \sim R_t^2 P_t \sim t^{2/z - \delta}$$

at criticality implies

$$y_R = 1/z. \quad (23)$$

To test these predictions, Fig. 7 shows log-log plots of  $t^{y_N} p_N(t, s)$  versus  $s/t^{y_N}$  and  $t^{y_R} p_R(t, s)$  versus  $s/t^{y_R}$ . The figures show bond DP data for the square lattice for  $d = 1$  and the BCC lattice for  $d = 4, 5$ . For  $d = 1$ , we set the exponents  $y_N$  and  $y_R$  to  $y_N = 0.47314$  and  $y_R = 0.63263$ , using the results from Table IX in Appendix A. For  $d = 4$  and  $5$ , the mean-field predictions  $y_N = 1$  and  $y_R = 1/2$  were used. In principle, logarithmic corrections should be taken into account for  $d = 4$ , however we did not pursue this here. The conjectures (20), (22) and (23) are strongly supported by the excellent data collapse observed in Fig. 7.



From Fig. 7, we observe that for  $s/t^{y_N}, s/t^{y_R} \ll 1$ , the curves appear to asymptote to a straight line. We find empirically that these slopes are well described by the expressions  $1/y_N - 1$  and  $1/y_R - 1 + d$ , for  $p_N(t, s)$  and  $p_R(t, s)$  respectively. We therefore conjecture that these expressions hold exactly, and we illustrate them with the dashed lines in Fig. 7. As a result, the scaling forms (20) can be recast as

$$\begin{aligned} p_N(t, s) &\sim t^{-1} s^{1/y_N - 1} f_N(s/t^{y_N}), \\ p_R(t, s) &\sim t^{-1 - d y_R} s^{1/y_R - 1 + d} f_R(s/t^{y_R}), \end{aligned} \quad (24)$$

with  $f_N$  and  $f_R$  universal.

## VI. DISCUSSION

We present a high-precision Monte Carlo study of bond and site DP on  $(d + 1)$ -dimensional simple-cubic and body-centered-cubic lattices, with  $2 \leq d \leq 7$ . A dimensionless ratio  $Q_t = N_{2t}/N_t$  constructed from the number of wet sites  $N_t$  is defined and used to estimate the critical thresholds. We report improved estimates of thresholds for  $2 \leq d \leq 7$ , and in high dimensions ( $d > 4$ ) we provide estimates of  $p_c$  in several cases for which no previous estimates appear to be known. In addition, we report improved estimates of the critical exponents for  $d = 2$  and 3. The accuracy of these estimates was due in part to the use of reduced-variance estimators introduced in [16, 19, 20]. At the estimated thresholds, we also conjecture, and numerically confirm, the finite-size scaling of the critical probability distributions  $p_N(t, s)$  and  $p_R(t, s)$ .

The high-precision Monte Carlo data reported in this work also suggests that further investigation of a number of questions is desirable. Firstly, is there an underlying physical reason (e.g. hidden symmetry) that in two and three dimensions bond DP on the BCC lattice suffers less finite-size corrections than site DP on the BCC lattice and both site and bond DP on the SC lattice? Second, can we obtain deeper understanding of origin of the scaling behavior described by (24)?

## VII. ACKNOWLEDGMENTS

We thank Peter Grassberger for helpful comments and for sharing code with us. J.F.W acknowledges the useful discussion with Wei Zhang. The simulations were carried out in part on NYU's ITS cluster, which is partly supported by NSF Grant No. PHY-0424082. In addition, this research was undertaken with the assistance of resources provided at the NCI National Facility through the National Computational Merit Allocation Scheme supported by the Australian Government. This work is supported by the National Nature Science Foundation of China under Grant No. 91024026 and 11275185, and the Chinese Academy of Sciences. It was also supported under the Australian Research Council's Discovery Projects

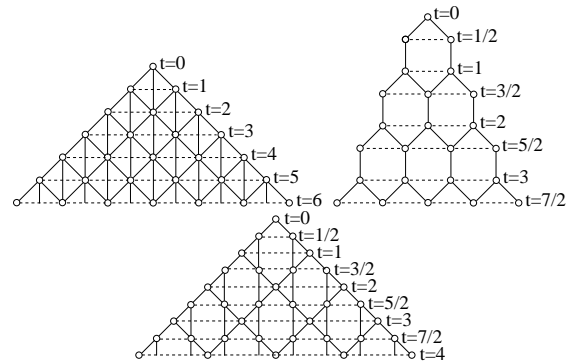


FIG. 8. Plots of triangular, honeycomb, and kagome lattices.

funding scheme (project number DP110101141), and T.G. is the recipient of an Australian Research Council Future Fellowship (project number FT100100494). J.F.W and Y.J.D also acknowledge the Specialized Research Fund for the Doctoral Program of Higher Education under Grant No. 20103402110053.

### Appendix A: Estimates of thresholds and critical exponents in (1+1) dimensions.

In this appendix we report estimates of the critical thresholds and critical exponents for a number of (1+1)-dimensional lattices. Specifically, we simulated bond and site DP on square (Fig. 1), triangular, honeycomb, and kagome lattices (Fig. 8). On the triangular lattice, a site at time  $t$  has three neighboring sites at times  $t' < t$ : two at  $t - 1$  and one at  $t - 2$ . On the honeycomb lattice, a site at an odd time  $t$  has two neighboring sites at time  $t - 1$ , while sites at even times have only one neighbor at time  $t - 1$ . On the kagome lattice, a site at an odd time  $t$  has one neighbour at time  $t - 1$  and one at time  $t - 2$ , while sites at even times have two neighbours at time  $t - 1$ .

The general methodology applied for these simulations is as described in Section II. However we did not apply the reduced-variance estimators in this case, since their variance only becomes suppressed in high dimensions. The thresholds estimated from  $Q_t$  for  $d = 1$  are shown in Table VIII. The estimates of the critical exponents are shown in Table IX. These estimate are consistent with, but less precise than, results obtained previously using series analysis.

### Appendix B: Discussion of the improved estimators

In this appendix we prove the identities (3) and (4). Both are direct consequences of the following lemma.

**Lemma 1.** *For both bond and site DP we have the following. If  $b_v$  is the number of Bernoulli trials required to determine the state of  $v \in V_t$  given the site configuration*

Lattice	Site		Bond	
	$p_c(\text{Present})$	$p_c(\text{Previous})$	$p_c(\text{Present})$	$p_c(\text{Previous})$
square	0.705 485 2(3)	0.705 485 22(4) [9] 0.705 489(4) [29]	0.644 700 1(2)	0.644 700 185(5) [9] 0.644 700 15(5) [8]
triangular	0.595 647 0(3)	0.595 646 75(10) [30] 0.595 646 8(5) [8]	0.478 025 0(4)	0.478 025 25(5) [30] 0.478 025(1) [8]
honeycomb	0.839 931 6(2)	0.839 933(5) [31]	0.822 856 9(2)	0.822 856 80(6) [30]
kagome	0.736 931 7(2)	0.736 931 82(4) [30]	0.658 968 9(2)	0.658 969 10(8) [30]

TABLE VIII. Estimates of thresholds in (1+1) dimensions on the square, triangular, honeycomb and kagome lattices.

	$\beta$	$\nu_{\parallel}$	$\nu_{\perp}$	$z$	$\theta$	$\delta$
Present	0.276 7(3)	1.735 5(15)	1.097 9(10)	1.580 7(2)	0.313 70(5)	0.159 44(2)
[9]	0.276 486(8)	1.733 847(6)	1.096 854(4)	1.580 745(10)	0.313 686(8)	0.159 464(6)

TABLE IX. Estimates of the critical exponents for  $d = 1$ .

at time  $t - 1$ , then

$$\mathbb{P}(s_v = 1) = p \langle b_v \rangle.$$

It follows immediately from Lemma 1 that for any set of constants  $a_v$  with  $v \in V_t$  we have

$$\left\langle \sum_{v \in V_t} a_v \delta_{s_v, 1} \right\rangle = p \left\langle \sum_{v \in V_t} a_v b_v \right\rangle, \quad (\text{B1})$$

where  $\delta_{\cdot, \cdot}$  denotes the Kronecker delta. Choosing  $a_v = 1$  in (B1) gives (3), while choosing  $a_v = r_v^2$  gives (4).

It now remains only to prove Lemma 1.

*Proof of Lemma 1.* For  $v \in V_t$ , let  $n_v$  denote the number of wet neighbours of  $v$  in  $V_{t-1}$ .

For site DP,

$$b_v = \begin{cases} 1, & \text{if } n_v > 0, \\ 0, & \text{if } n_v = 0, \end{cases}$$

and so  $\langle b_v \rangle = \mathbb{P}(n_v > 0)$ . Since  $\mathbb{P}(s_v = 1) = p \mathbb{P}(n_v > 0)$ , the stated result then follows.

For bond DP, the situation is more involved. Since  $\mathbb{P}(s_v = 1) = \langle 1 - (1 - p)^{n_v} \rangle$ , our task is to establish

$$p \langle b_v \rangle = \langle 1 - (1 - p)^{n_v} \rangle. \quad (\text{B2})$$

If we consider a fixed value of  $n_v$  then consideration of the stochastic process defined in Section II A shows that

$$\begin{aligned} \mathbb{E}(b_v | n_v) &= \sum_{k=1}^{n_v-1} k(1-p)^{k-1}p + n_v(1-p)^{n_v-1} \\ &= \frac{1}{p}(1 - (1-p)^{n_v}). \end{aligned} \quad (\text{B3})$$

From (B3) Taking the expectation of (B3) yields (B2), which concludes the proof.  $\square$

- 
- [1] S. R. Broadbent and J. M. Hammersley, Proceedings of the Cambridge Philosophical Society **53**, 629 (1957).  
[2] E. V. Albano, J. Phys. A **27**, L881 (1994).  
[3] D. Mollison, J. R. Stat. Soc. Ser. B (Methodol) **39**, 283 (1977).  
[4] J.-P. Bouchaud and A. Georges, Phys. Rep. **195**, 127 (1990).  
[5] S. Havlin and D. Benavraham, Adv. Phys. **36**, 695 (1987).  
[6] H.-K. Janssen, Z. Phys. B **42**, 151 (1981).  
[7] P. Grassberger, Z. Phys. B **47**, 365 (1982).  
[8] I. Jensen, J. Phys. A **29**, 7013 (1996).  
[9] I. Jensen, J. Phys. A **32**, 5233 (1999).  
[10] P. Grassberger and Y. Zhang, physica A **224**, 169 (1996).  
[11] P. Grassberger, J. Stat. Mech.: Theory Exp., P08021 (2009).  
[12] E. Perlsman and S. Havlin, Europhys. Lett. **58**, 176 (2002).  
[13] S. Lubeck and R. Willmann, J. Stat. Phys. **115**, 1231 (2004).  
[14] J. Adler, J. Berger, J. A. M. S. Duarte, and Y. Meir, Phys. Rev. B **37**, 7529 (1988).  
[15] J. Blease, J. Phys. C **10**, 917 (1977).  
[16] P. Grassberger, Phys. Rev. E **79**, 052104 (2009).  
[17] We note that the version of bond DP that we are simulating generates a different ensemble of bond configurations compared to the standard geometric version of bond DP, in which each edge is occupied independently. However, the resulting site configurations generated by these two bond DP models are identical. Since we only consider properties of the site configurations in this article, the distinction is unimportant for our purposes. For the sake

of computational efficiency, we find the version described in the text more convenient.

- [18] R. Sedgewick, *Algorithms in C*, 3rd ed. (Addison-Wesley, Reading, Massachusetts, 1998).
- [19] P. Grassberger, Phys. Rev. E **67**, 036101 (2003).
- [20] J. G. Foster, P. Grassberger, and M. Paczuski, New J. Phys. **11**, 023009 (2009).
- [21] R. Dickman, Phys. Rev. E **60**, R2441 (1999).
- [22] H.-K. Janssen and U. Täuber, Ann. Phys. **315**, 147 (2005).
- [23] H.-K. Janssen and O. Stenull, Phys. Rev. E **69**, 016125 (2004).
- [24] H. Hinrichsen, Adv. Phys. **49**, 815 (2000).
- [25] C. Kurrer and K. Schulten, Phys. Rev. E **48**, 614 (1993).
- [26] J. Bronzan and J. Dash, Phys. Lett. B **51**, 496 (1974).
- [27] C. A. Voigt and R. M. Ziff, Phys. Rev. E **56**, R6241 (1997).
- [28] I. Jensen, Phys. Rev. A **45**, R563 (1992).
- [29] S. Lubeck and R. Willmann, J. Phys. A **35**, 10205 (2002).
- [30] I. Jensen, J. Phys. A **37**, 6899 (2004).
- [31] I. Jensen and A. Guttmann, J. Phys. A **28**, 4813 (1995).